nuclear fusion
IAEA

PAPER • OPEN ACCESS

Non-linear MHD investigations of high-confinement regimes without type-I ELMs in ASDEX Upgrade and JT-60SA

To cite this article: A. Cathey *et al* 2024 *Nucl. Fusion* **64** 096003

View the article online for updates and enhancements.

You may also like

- Analysis and expansion of the quasi-continuous exhaust (QCE) regime in ASDEX Upgrade
M. Faitsch, T. Eich, G.F. Harrer et al.
- Thin-body effects in double-gate tunnel field-effect transistors
Nguyen Dang Chien, Bui Huu Thai and Chun-Hsing Shih
- Developing a physics understanding of the quasi-continuous exhaust regime: pedestal profile and ballooning stability analysis
L. Radovanovic, M. Dunne, E. Wolfrum et al.

This content was downloaded from IP address 150.214.182.235 on 27/08/2024 at 10:27

OPEN ACCESS
IOP Publishing | International Atomic Energy Agency
Nuclear Fusion
Nucl. Fusion **64** (2024) 096003 (12pp)
https://doi.org/10.1088/1741-4326/ad5e97

Non-linear MHD investigations of high-confinement regimes without type-I ELMs in ASDEX Upgrade and JT-60SA

A. Cathey[1,*], M. Hoelzl[1], L. Meier[2], M.G. Dunne[1], G.T.A. Huijsmans[3], L. Gil[4], G.F. Harrer[5], N. Aiba[6], D.J. Cruz-Zabala[7], K. Lackner[1], S.J.P. Pamela[8], E. Viezzer[7], E. Wolfrum[1], S. Günter[1], the JOREK Team[a], the ASDEX Upgrade Team[b], and the EUROfusion WPTE Team[c]

[1] Max Planck Institute for Plasma Physics, Boltzmannstr.2, 85748 Garching, Germany
[2] Eindhoven University of Technology, PO Box 513, 5600 MB Eindhoven, Netherlands
[3] CEA, IRFM, 13108 Saint-Paul-Lez-Durance, France
[4] Instituto de Plasmas e Fusão Nuclear, Instituto Superior Técnico, Universidade de Lisboa, 1049-001 Lisboa, Portugal
[5] Institute of Applied Physics, TU Wien, 1040 Vienna, Austria
[6] National Institutes for Quantum Science and Technology, Naka, Japan
[7] University of Sevilla, Sevilla, Spain
[8] CCFE, Culham Science Centre, Abingdon, Oxon OX14 3DB, United Kingdom of Great Britain and Northern Ireland

E-mail: andres.cathey@ipp.mpg.de

Received 25 January 2024, revised 6 June 2024
Accepted for publication 3 July 2024
Published 18 July 2024

Abstract

Large edge localised modes (ELMs) would cause an unacceptable reduction of material lifetime in future large tokamaks due to the significant amount of energy expelled from the magnetically confined region towards the plasma facing components. Thoroughly validated modelling of regimes devoid of large ELMs is crucial as it may then provide predictive insights prior to tokamak operation and design. This paper describes recent efforts pursued with the non-linear extended MHD code JOREK in the modelling of three scenarios without large ELMs: quiescent H-mode (QH-mode), quasi-continuous exhaust regime (QCE regime), and the enhanced D-alpha H-mode (EDA H-mode). For each of these regimes, the non-linear dynamics observed in the simulations are detailed and compared to experimental observations of the underlying instabilities of each regime (edge harmonic oscillation for QH-mode, small ELMs for QCE regime, and quasi-coherent mode for EDA H-mode). For QH-mode, the kink-peeling mode is found to govern the dynamics and a transition to a large ELM is obtained above the same density threshold as in the modelled experiment. For the QCE regime and EDA H-mode, resistive peeling–ballooning modes dominate and pedestal fluctuation frequencies correspond well to experimental observations. The dominant mechanisms for the excitation and suppression

[a] See Hoelzl *et al* 2024 (https://doi.org/10.1088/1741-4326/ad5a21) for the JOREK Team.
[b] See Zohm *et al* 2024 (https://doi.org/10.1088/1741-4326/ad249d) for the ASDEX Upgrade Team.
[c] See Joffrin *et al* 2024 (https://doi.org/10.1088/1741-4326/ad2be4) for the EUROfusion WPTE Team.
[*] Author to whom any correspondence should be addressed.

Original Content from this work may be used under the terms of the Creative Commons Attribution 4.0 licence. Any further distribution of this work must maintain attribution to the author(s) and the title of the work, journal citation and DOI.

 © 2024 The Author(s). Published by IOP Publishing Ltd on behalf of the IAEA

of these instabilities are presented and their influence on simulation dynamics is shown. Finally, predictive simulations of edge instabilities at different values of plasma resistivity in a 4.60 MA scenario with low edge safety factor in JT-60SA are presented.

Keywords: non-linear MHD, edge localised modes, peeling–ballooning modes, pedestal physics

(Some figures may appear in colour only in the online journal)

1. Introduction

Understanding and controlling edge localised modes (ELMs) in high-confinement regime (H-mode) has become a central focus of research in the field of plasma physics and magnetic confinement fusion, as it promises enhanced performance without the intolerable heat loads associated to unmitigated ELMs [1]. ELMs are repetitive perturbations of the outermost confined plasma (the so-called 'pedestal') in standard high-confinement mode (H-mode). They are destabilised by large pedestal pressure and plasma current (and their gradients) and expel between 5% and 15% of the plasma stored energy [2, 3]. Because this process occurs in time scales between 0.5 and 3 milliseconds, ELMs result in potentially intolerable heat and particle loads to plasma facing components of reactor-relevant devices [4]. Several H-mode regimes of operation manage to actively and naturally avoid large ELMs from appearing. Active ELM control strategies include magnetic perturbations and pellet pacing, which are foreseen to be applied in ITER, but it is presently still unclear at which parameter regimes these will be viable alternatives [5]. On the other hand, natural ELM-free H-modes that exhibit small/no-ELM activity constitute an additional alternative to operate without the deleterious ELMs and maintain the benefits of H-mode (enhanced density, temperature, and energy confinement of the core plasma which all translates to more fusion power). Naturally ELM-free H-modes emerge without active control schemes, albeit in narrow operational windows. For these ELM-free H-modes, the transient relaxation process caused by ELMs is replaced by a different transport mechanism in order to maintain an edge pedestal which does not give rise to large ELMs. However, like active ELM control, each ELM-free regime exists in specific operational spaces in present-day devices, and their extrapolation to ITER (or any other future device) cannot be precisely determined. Improving the understanding of naturally ELM-free regimes through non-linear simulations could provide a path for predicting ELM-free regimes of operation in ITER and beyond.

At the ASDEX Upgrade tokamak (AUG), small/no-ELM regimes such as the quiescent H-mode (QH-mode), quasi-continuous exhaust regime (QCE regime), and enhanced D-alpha H-mode (EDA H-mode) are actively investigated to understand whether they could be relevant for ITER. Despite being accessible when the device had a carbon wall, QH-mode in AUG could not be obtained for several years after changing to a full tungsten wall [6]. Other devices like JET (with carbon wall only), JT-60U, and DIII-D have achieved QH-mode operation, with the latter being the first device in which QH-mode had been observed [7]. The QCE regime has been an active research topic in AUG (previously called small ELMs and, before that, type-II ELMs), TCV [8] and, during the course of last year, in JET-ILW [9]. The EDA H-mode, which was first observed in Alcator C-mod [10], has been then reproduced in EAST [11], AUG (with tungsten wall) [12] and, recently, in JET-ILW [9]. Presently, first-principles understanding of these regimes is missing due to the complex and non-linear physical processes involved together with large uncertainties in experimental measurements. Numerical modelling and simulations play a complimentary role in these efforts and significant progress has been achieved in recent years with several different models and codes. Modelling of active ELM control are also pursued with JOREK (pellet-triggering of ELMs [13, 14] the application of resonant magnetic perturbations [15, 16] and vertical kicks [17]).

In recent years, significant progress has been achieved with JOREK regarding simulations of ELMs and ELM-free regimes. JOREK is a 3D non-linear extended MHD code [18, 19] that has been at the forefront of efforts to investigate the dynamics of ELMs and understand the underlying physics that govern their behaviour in tokamak plasmas. The physics of the pedestal is studied with JOREK modelling of scenarios that are characterised by natural ELMs, RMP-mitigation and suppression, pellet-triggered ELMs, as well as small/no-ELM regimes. The importance of resistivity and plasma flows in the physical mechanism of natural ELM triggering has been investigated with JOREK under the scope of simulations of single ELMs and, more recently, repetitive ELM cycles [20–22]. Beyond the ELM-trigger mechanism, resistivity also plays a critical role in pedestal stability and its non-linear dynamics during the ELM crash, for RMP penetration and island formation, and also for small/no-ELM regimes.

In this paper, the progress regarding simulations of naturally ELM-free H-mode regimes (small/no-ELM regimes) in AUG using the JOREK code is described. A comparative review of JOREK simulations of H-mode regimes without large ELMs in the ASDEX Upgrade tokamak is presented first and it is followed by simulations of JT-60SA. In section 2, experimental characteristics of three naturally ELM-free regimes (QH-mode, QCE regime, and EDA H-mode) are presented. In section 3, a description of the reduced MHD model in JOREK, as well as simulation set-ups and results for each of these regimes are shown and contrasted to each other. In section 4, JOREK simulations of pedestal stability of a JT-60SA scenario with 4.6 MA are shown. Finally, section 5 includes concluding remarks and key takeaways.

Table 1. Parameter space for different AUG discharges with small/no-ELM regimes under investigation.

Regime	δ (up/down)	$q_{\psi_{\text{norm}}=0.95}$	β_{pol}	$\nu_{*e,95}$	$n_{e,95}$	$T_{e,95}$
QH-mode	0.38 (0.31/0.44)	6.8	1.50	0.43	$1.74 \times 10^{19}\,\text{m}^{-3}$	831 eV
Small ELMs	0.24 (0.08/0.40)	5.4	0.69	6.42	$4.52 \times 10^{19}\,\text{m}^{-3}$	281 eV
EDA H-mode	0.41 (0.32/0.49)	5.3	0.91	6.64	$6.70 \times 10^{19}\,\text{m}^{-3}$	328 eV

2. Phenomenology of small/no-ELM regimes

The present section gives an overview of experimental observations relating to QH-mode 2.1, QCE regime 2.2, and EDA H-mode 2.3. Key aspects to take into consideration regarding small/no-ELM regimes are the access window (operational conditions) and the physical mechanism that regulates the pedestal in the absence of ELMs. In the absence of such mechanism, ELM-free regimes are observed to be non-stationary phases and, as such, are not reactor relevant. Large ELMs appear when the so-called peeling–ballooning (PB) boundary is crossed by operating at a sufficiently large normalised pressure gradient and/or with a sufficiently large current density at the pedestal. For the former, the excitation of ELMs with dominant high toroidal mode numbers (ballooning-dominated) takes place, while for the latter, peeling-dominated ELMs are observed (dominant low toroidal mode numbers).

In order to keep a good overview of the differences between the three regimes, table 1 shows, the average (of upper and lower) triangularity, edge safety factor, β_{pol}, electron pedestal collisionality, density and temperature. It is reiterated here that the QH-mode discharge was performed with an upper single null and with the unfavourable grad B drift configuration. The small ELMs and EDA H-mode had a lower single null and favourable grad B drift configuration. The former uses a lower triangularity than the QCE regime.

2.1. QH-mode

Near the boundary of peeling stability, within a parameter regime featuring high bootstrap current (typically at low densities in present-day devices), QH-mode can be achieved. An edge harmonic oscillation (EHO) induces heat and particle transport across the plasma pedestal and is a salient characteristic of well-established QH-mode. The EHO maintains pedestal gradients below the threshold for edge localized modes (ELMs), consequently preventing large ELMs from becoming destabilised. Low toroidal mode numbers (n 1 . . . 3) alongside multiple higher harmonics are typical features of the EHO [23]. This edge perturbation that interacts with the bulk plasma is postulated to result from a saturated kink/peeling instability, driven by the strong bootstrap current density, enabling the plasma to attain an ELM-free, quasi-stable condition [24]. Initially demonstrated in the DIII-D tokamak under conditions of low pedestal density and strong counter-current neutral beam injection (NBI), the accessibility region for QH-mode was subsequently broadened to co-current NBI and without NBI. Although QH-mode is typically lost at high pedestal densities across various devices, experiments at DIII-D have achieved QH-mode at higher $n_{e,\text{ped}}$ by carefully shaping the magnetic configuration [25]. The key for consistent QH-mode access seems to be the presence of a suitably sheared ExB flow coupled with a pedestal that lies close to, but not over, the peeling stability boundary. This boundary is commonly found at low pedestal collisionality, correlating with low pedestal density in contemporary devices. Simulations of QH-mode across different devices have been reported with MHD codes like JOREK [26, 27], NIMROD [28, 29], and BOUT++ [30].

At the full tungsten AUG, transient QH-mode operation has been recently achieved with an unfavourable ion grad B drift configuration [6]. The stationary establishment of QH-mode in a device with a full tungsten wall is challenging compared to carbon-walled devices (like DIII-D) for mainly two reasons. It is not possible to operate without a gas puff altogether, which increases the pedestal density and, therefore, collisionality. And secondly, core ECRH is needed to avert tungsten accumulation in the plasma core, which results in elevated Te relative to Ti and makes achieving QH-mode more intricate. At AUG-W, QH-mode has now been achieved in two configurations: a lower single null configuration with reversed field (counter-current NBI) and an upper single null, forward field configuration (co-current NBI). Discharge #39279 with upper single null is used to prepare the simulations presented in this contribution (and thoroughly described in [31]). Operating in a forward field configuration, this discharge sustained QH-mode for around 150 ms within the time range of 3.44 s–3.59 s. With a positive plasma current of 0.6 MA (considering the positive direction as counter-clockwise when viewed from above) and co-current NBI, the discharge featured a toroidal magnetic field of -2.5 T. The magnetic configuration, shown in figure 1(right), is close to a double null: an elongation of $\kappa = 1.83$, upper triangularity of $\delta_{\text{upper}} = 0.44$, and $\delta_{\text{lower}} = 0.31$.

The AUG discharge was mostly beam heated with beam blips of incrementally longer duration applied after 3.4 s. Time traces of heating power, thermal energy, two interferometer lines-of-sight, and a spectrogram for a magnetic pick-up coil situated at the outboard midplane are shown in figure 1(left). A transient QH-mode phase during which an EHO characterised by an $n = 1$ toroidal mode number with several harmonics is present for roughly 0.15 s. The EHO fundamental frequency is around 10 kHz and it is lost when the pedestal density increases beyond a given threshold value—the density increase takes place due to the absence of a pump in the upper divertor, the progressive increase in NBI power, and an insufficient particle transport caused by the EHO. In section 3.1, JOREK simulations for this discharge are described.

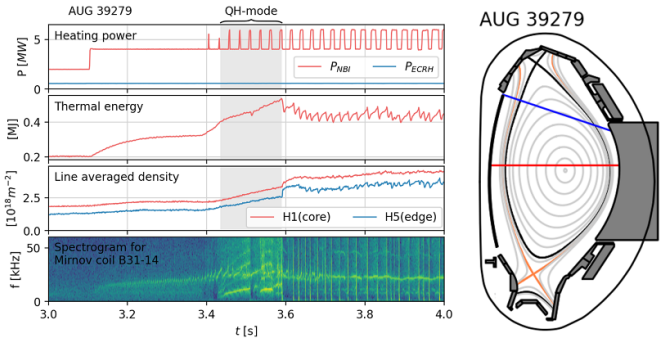

Figure 1. AUG #39279 with QH-mode phase used as initial conditions for JOREK simulations. (left) From top to bottom: heating power, stored thermal energy, line-integrated density for two lines of sight, spectrogram of magnetic pick-up coil B31-14. (right) Magnetic geometry showing primary and secondary separatrices as well as the H1 and H5 interferometer lines-of-sight.

2.2. QCE regime

Small ELM regimes that avoid large ELMs include the QCE regime, grassy ELMs [32], type-III ELMs (not strictly reactor-relevant due to their negative impact on confinement [33]), and a recently-observed small ELM regime at low $n_{e,ped}$ in JET [34]. The QCE regime can maintain favourable confinement properties at strong shaping (high triangularity and elongation) and was previously referred to as type-II ELMs or small ELMs. In addition to strong shaping, which allows good confinement, high $n_{e,sep}$ (achieved with strong gas puffing) is needed to achieve the QCE regime; concretely, $n_{e,sep} > 0.3n_{GW}$ has been reported [8]. High-n ballooning modes near the separatrix are hypothesised to produce the necessary (heat and particle) transport to keep the pedestal below the type-I stability boundary [35]. One important characteristic of the QCE regime is that the power fall-off length is observed to be larger than predictions based on the empirical Eich scaling [36]. The underlying edge perturbations that replace large ELMs in the QCE regime are also present when $n_{e,sep} > 0.3n_{GW}$, but the magnetic configuration hosts lower triangularity and/or elongation. Under these circumstances, however, the small ELMs are observed to be larger and confinement degradation (H-factor smaller than 1) is ubiquitous. For such small ELMs at low triangularity, JOREK has been used in order to characterise the underlying instabilities [37].

2.3. EDA H-mode

The EDA H-mode features an electromagnetic quasi-coherent mode (QCM) localized on the low-field side within the steep gradient region of the pedestal. In AUG, the QCM frequency range is $f_{QCM} = 15 \ldots 40\,\text{kHz}$, moves in the electron diamagnetic direction (laboratory frame), and has been estimated to have toroidal mode numbers of $n \sim 10$–20 [12]. Generally, the QCM is easily visible in spectrograms of various local (or line-integrated) diagnostics like interferometers, electron cyclotron emission (ECE), thermal He beam and, sometimes, on one or more magnetic pick-up coils (coils closest to the plasma measure the QCM more easily) and it has been studied directly with probes [38]. In AUG, the EDA H-mode was first obtained with ECRH only inside a narrow power window that broadens with stronger shaping (larger triangularity and elongation). Notably, a QCM is also sometimes observed during the QCE regime in AUG, but featuring broader frequency peaks [39], which acts an indicator of a certain connection between the EDA H-mode and the QCE regime.

Experimental discharges without NBI heating cannot provide measurements of the ion temperature, which motivated extending the EDA H-mode towards also (partially) beam heated plasmas [40]. One of such discharges is used to obtain the initial conditions used to prepare and run non-linear JOREK simulations. AUG discharge #36330 (-2.5 T and 0.8 MA) has an even mix of NBI and ECRH totalling to 5 MW with additional argon seeding (seeding rate was feedback-controlled to maintain a fixed $P_{sep} = P_{heat} - P_{rad} = 1.5\,\text{MW}$; see figure 2(top left) in [40]) and displays a controlled EDA H-mode phase that is stationary during several seconds with a QCM visible at $f \sim 30$ kHz. The magnetic geometry is lower single-null with high triangularity and elongation ($\delta_{upper} = 0.31$, $\delta_{lower} = 0.49$, and $\kappa = 1.6$) in the favourable grad B drift configuration. The profiles that are obtained from the experimental data together with error bars (Thompson scattering for Te and ne and CXRS for Ti) to start the JOREK simulations are shown in figure 2(left). The discrepancy between the fitted Er profile to CXRS measurements and the input to JOREK (black crosses) results from the simplification of considering a single temperature model instead of separate Te and Ti, and the absence of a toroidal rotation source to include the NBI torque. This influences the stability of PB modes, specially of intermediate and high toroidal mode numbers and, therefore, is an avenue for future work. The operational point with respect to the ideal linear MHD PB boundary is shown in figure 2(right). From the MISHKA-1 analysis, it is clear that the operational point lies close to the $n \sim 14$ ballooning boundary, however this neglects the stabilising influence of diamagnetic and ExB flows [41].

3. JOREK simulations of small/no-ELM regimes in AUG

This section details the non-linear extended MHD JOREK simulation results for the three different small/no-ELM regimes under consideration throughout this paper. In section 3.1, a description of the reduced MHD model with diamagnetic extension that is used for all simulations presented here is provided. Distinct similarities are clearly observed between EDA H-mode and small ELMs at low triangularity. And important differences are found between QH-mode and EDA H-mode. A description of the simulations for QH-mode is detailed in section 3.2, followed by small ELMs at low triangularity in section 3.3, and EDA H-mode in section 3.4. Finally, section 3.5 describes the most important similarities and differences between the three small/no-ELM regimes in terms of the simulation results and characteristics of the observed non-axisymmetric perturbations and their dynamics.

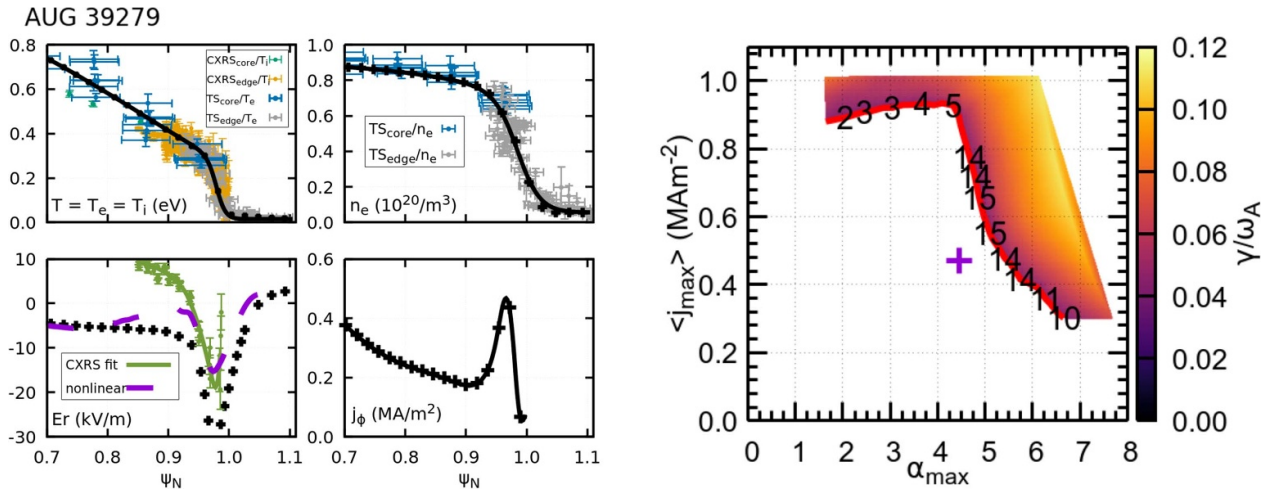

Figure 2. AUG #36330 with EDA H-mode phase used as initial conditions for JOREK simulations. (left) Profiles together with measurements and uncertainties of temperature (Te and Ti), density, radial electric field (black is the profile in the linear phase, purple during the non-linear phase, and in green the CXRS data and fit), and current density. (right) MISHKA-1 linear ideal MHD analysis showing the operational point close to the n 14 ballooning boundary.

3.1. JOREK reduced MHD model

The JOREK code solves the visco-resistive MHD equations either with a full MHD or reduced MHD model, and it is rigorously described in [18, 19]. The reduced MHD model consists of two assumptions that reduce the number of unknowns from 8 (scalar equations: continuity equation and adiabatic pressure equation, vectorial equations: electromagnetic vector potential, and ion momentum equation) to 5 (scalar equations: continuity, pressure, poloidal magnetic flux, electrostatic potential, parallel velocity). The assumptions are that the toroidal magnetic field (which is effectively determined by the toroidal field coils) is stationary and that the ExB velocity is considered to be on the poloidal plane. The assumption of stationary toroidal magnetic field simultaneously eliminates one dynamic variable and the fast magnetosonic wave from the system. The expressions of the velocity can include an extension to account for diamagnetic drifts, which allows the pedestal E_r well (characteristic of the H-mode pedestal) to be self-consistently included in the simulations[9]. The associated ExB flow and the diamagnetic flow have an important effect on the stability of PB modes (ideal and resistive alike), such that including them in the simulation is crucial [42, 43]. The presence of this radial electric field has important consequences regarding the stability of the underlying instabilities that give rise to ELMs [44]. After these considerations are made, the magnetic field and the velocity may be written as

$$\boldsymbol{B} = \frac{F_0}{R}\hat{\varphi} + B_{\mathrm{pol}}\hat{\vartheta}, \text{ where } B_{\mathrm{pol}} = \frac{1}{R}\nabla\psi \times \hat{\varphi}, \text{ and}$$

$$\boldsymbol{v} = v_{\parallel}\frac{\boldsymbol{B}}{|B|} + v_{\mathrm{ExB}}\hat{\vartheta} + \boldsymbol{v}_{\mathrm{dia,i}},$$

$$\text{with } \boldsymbol{v}_{\mathrm{dia,i}} = -\frac{R\nabla p_i \times \hat{\varphi}}{e m_{\mathrm{ion}} F_0 n_e} = -\frac{\delta^* R}{m_e n_e}\nabla p_i \times \hat{\varphi}.$$

Making use of such assumptions and including diffusive particle and heat transport, the visco-resistive MHD equations turn into the reduced MHD equations in JOREK (detailed in [18]). The resistivity profile that is used corresponds to the Spitzer dependency, $\eta \sim T^{-3/2}$. Parallel heat transport can be treated at realistic parallel-to-perpendicular heat asymmetry and the Spitzer-Härm expression is used in the code ($\chi_{\parallel} \sim T^{5/2}$). Perpendicular diffusion of heat and particles are included with *ad-hoc* profiles, which act as substitute for anomalous transport that requires non-linear gyro-kinetic modelling to treat appropriately. Each scenario presented in the following uses a specific set of diffusion and source profiles (which is kept stationary in time) tailored to ensure a certain evolution of the pedestal in the absence of any perturbations. As a result, when introducing non-axisymmetric perturbations, any additional transport channel is coming from any non-linear mode activity. In addition to the diamagnetic drift extension which goes directly to the velocity representation, an extension to include the neoclassical bootstrap current (which becomes stronger upon steepening of the density/temperature/pressure profiles) is also present in the JOREK code. This is included through a source term (determined by the analytical Sauter formula [45, 46]) in the induction equation such that the build-up of the current density resulting from an increase in the bootstrap current takes place in the resistive time scales. The current source term includes the bootstrap and Ohmic contributions with a Krook operator, $\eta(j - j_{\mathrm{src}})$. Both the diamagnetic drift and the bootstrap current extensions to the reduced MHD equations are used for the simulations presented in this paper. Higher order finite Larmor radius effects are not considered for the simulations presented here. BOUT++ simulations that delve into the influence of such higher order FLR effects for the wide-pedestal QH-mode in DIII-D are discussed in [30]. In the following sections, the

[9] Parallel velocity can also influence the formation of E_r. In the modelling presented here, $v_{\parallel}$ is set solely by Mach-1 boundary conditions enforced at the simplified divertor targets. Including parallel momentum sources and understanding their effect is the topic of ongoing work.

three small/no-ELM regimes at AUG simulated with JOREK are described and compared.

3.2. QH-mode

JOREK has been used to simulate QH-mode in DIII-D [26] and preliminary simulations for ITER [27]. In both studies, the effect of diamagnetic flows were neglected. For QH-mode in AUG #39279, JOREK simulations including non-axisymmetric perturbations with $n = 1, 2, 3, \ldots, 6$ are shown. There are only two linearly unstable modes: $n = 1$ and 2 ($n = 2$ has a higher growth rate, but $n = 1$ ultimately becomes the dominant mode) as depicted with the magnetic energies of the different toroidal mode numbers shown in figure 3(top). During the non-linear phase, an $n = 1$ dominated kink-peeling mode is observed at a saturated state with all higher-n harmonics also present and visible in the non-sinusoidal perturbations of the plasma density and a frequency spectrogram of the perturbations at the pedestal, as shown in figure 3(bottom). The density perturbations used for the spectrogram were picked at a point in the outer midplane and exhibit strongest ($n = 1$) fluctuations at $f \approx 27$ kHz with the higher harmonics at multiples (corresponding to the higher toroidal mode numbers) of this fundamental frequency, which is higher than the frequency observed for the EHO in the discharge. In the experiment, the QH-phase exists during a phase where the beam blips are progressively increasing in duration, but the associated toroidal torque and the separation between electron and ion temperature were not included in the modelling at this stage, which likely explains why the kink-peeling mode does not match in frequency with the experiment.

The discharge modelled for this QH-phase simulation exhibited a transition towards type-I ELMs when $n_{\mathrm{e,ped}}$ increases beyond $\sim 2.3 \times 10^{19}\ \mathrm{m}^{-3}$, see figure 1(left). Taking the simulation from figure 3 at $t = 20$ms, the particle source is increased to study the EHO behaviour at higher densities and a transition to a type-I ELM is observed at the same density threshold as seen in AUG discharge #39279. The ELM that is simulated under these conditions is not fully resolved since the toroidal mode numbers included in the simulation ($n = 0, 1, \ldots, 6$) described the EHO dynamics well, but not that of a violent ELM crash, as the focus lies on the QH study[10]. The QH-mode was also probed at different values of the edge safety factor (by rigidly rising the q profile with an increase of the overall toroidal magnetic field such that the magnetic shear was kept unchanged) and clear access windows in q_{95} were observed, as expected from experimental results from AUG with a carbon wall [47]. The non-linear evolution of q_{95} is also found to contribute to the kink mode saturation.

[10] A simulation with twice as many toroidal harmonics showed the EHO to be unchanged, but the ELM crash onset would not be affected by increasing toroidal resolution. A change in the resulting ELM dynamics could be expected, as discussed in [22].

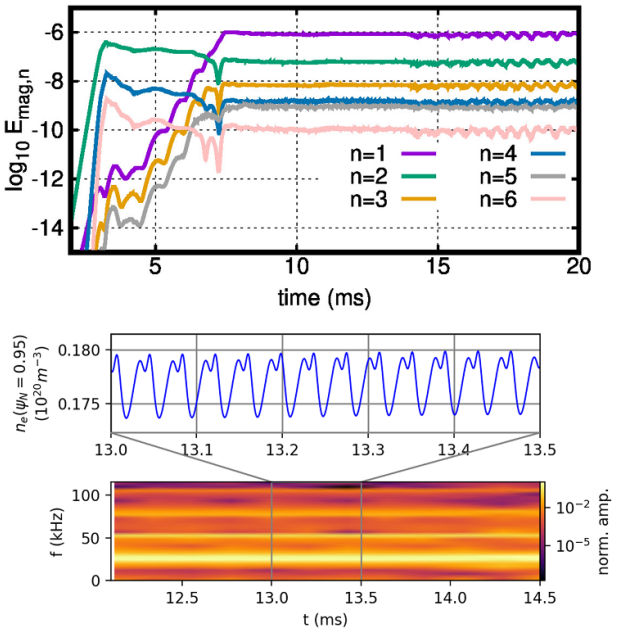

Figure 3. QH-mode: non-axisymmetric magnetic energies of perturbations with different toroidal mode numbers during a simulation using initial conditions from AUG #39279. An $n = 1$ dominant kink-peeling mode with higher-n harmonics is observed to saturate and is qualitatively consistent with an EHO. Density perturbations caused by the EHO at the pedestal in the low-field side. Frequency spectrogram of the density perturbations showing a dominant $n = 1$ fluctuation with $f \approx 27$ kHz together with the harmonics of higher toroidal mode numbers and frequencies.

3.3. Small ELMs at low triangularity

Direct simulations of an experimental discharge that features small ELMs associated to a QCE regime have not been performed with JOREK so far. However, small ELMs at low triangularity share several important features found in the QCE regime and are thus studied in the following (high δ modelling with JOREK are left for future work) by considering an AUG type-I ELMy discharge where $n_{\mathrm{e,sep}}$ is artificially increased until quasi-continuous activity develops and prevents type-I ELMs from becoming destabilised. These simulations have been presented in detail in [37]. The non-linear modelling includes all even toroidal mode numbers between $n = 0$ and 12 (simulations going until $n = 20$ show the same dynamics) and displays a quasi-continuous regulation of the pedestal such that type-I ELMs are not excited. The frequency of the perturbations observed in these small ELM simulations is around $20 - 40$ kHz measured at the steep gradient region in the outer midplane, which is qualitatively similar to QCE observations in AUG [39, 48]. The linearly unstable modes found in the simulation (as well as those which are non-linearly destabilised) are located near the separatrix with dominant toroidal mode numbers $n = 8$ and 10. These are identified as resistive PB modes since they are strongly affected by the local plasma resistivity and their velocity corresponds to that of resistive PB modes.

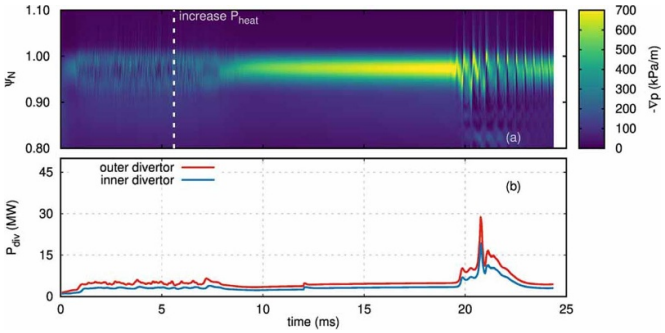

Figure 4. Small ELMs suppressed by increased heating power lead to pressure build-up and type-I ELMs. (*a*) pressure gradient across the pedestal over time and (*b*) inner/outer divertor incident power. Increasing heating power suppresses small ELMs and leads to the appearance of a type-I ELM at around 20 ms. Reproduced from [37]. © 2022 Max-Planck-Institut fur Plasmaphysik. CC BY 4.0.

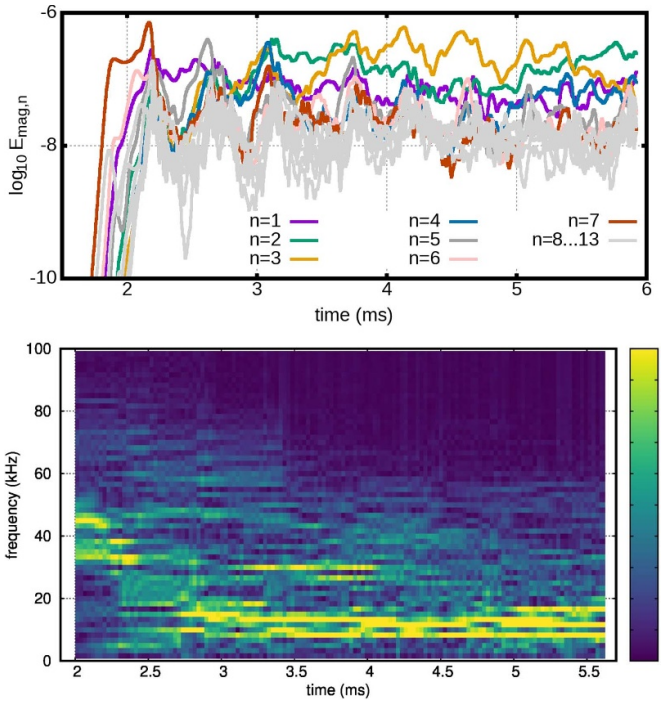

Figure 5. EDA H-mode: (top) non-axisymmetric magnetic energies of perturbations with different toroidal mode numbers during a simulation using initial conditions from AUG #36330. (bottom) spectrogram of pedestal fluctuations with f 13 kHz during the non-linear phase. Initially, fluctuations have higher frequencies until the Er profile is non-linearly modified. Adapted from [41]. © EURATOM 2023. CC BY 4.0.

In experimental characterisations of the QCE regime, it has been observed that separatrix density plays a pivotal role in the access to the regime and that only above $\approx 0.3 \times n_{GW}$ is the small ELM regime accessible [8]. This is tested in the simulations by comparing two cases with different values of density at the separatrix, and it is found that decreasing $n_{e,sep}$ leads to a suppression of the small ELMs and towards a type-I ELM crash (in the absence of small ELMs, the pedestal steepens until the type-I ELM is excited). Alternatively, it is also found that increasing the heating power (P_{heat}) leads to suppression of small ELMs and to the onset of a type-I ELM once the pedestal top increases sufficiently. Such behaviour takes place despite the associated steepening of the destabilising pressure gradient for two reasons. The increased heating power causes an increase of temperature that leads to a local reduction of the plasma resistivity ($\eta \propto T^{-3/2}$) which reduces some of the drive for these resistive PBM, and to an increase of the diamagnetic and ExB flow (through the steepening of ∇p) which has a stabilising effect on medium and high-n ballooning modes. Figure 4 shows how a simulation sustaining small ELMs transitions towards a type-I ELM a few milliseconds after the heating power is increased. In the figure, the top panel shows the outboard midplane pressure gradient which is characterised by rapid oscillations which become suppressed within a few milliseconds from the increase of P_{heat}. This is followed by a phase without any non-axisymmetric activity that abruptly comes to an end when a type-I ELM is excited at $\sim$20 ms. The inner and outer divertor incident power caused by the small ELMs and, eventually, the type-I ELM are shown in the bottom panel of the figure. A visual depiction of the evolving profiles can be seen in figure 18 from [37].

3.4. EDA H-mode

The simulations performed based on the experimental discharge described in section 2.3 are described in detail in [41] and contextualised in this section to portray them with respect to the simulations of QH-mode and small ELMs at low triangularity described in the previous two sections. The non-axisymmetric simulations include all toroidal modes between $n = 0$ and 13 and show linear growth of modes dominated by $n = \{6 \ldots 9\}$. Successively, linearly stable modes become non-linearly driven, and the collective perturbation displays fluctuation frequencies in the pedestal ranging around $\{8 \ldots 18\}$ kHz, exhibiting dominant resistive PB modes. The magnetic energies of the non-axisymmetric perturbations as well as a spectrogram of the temperature perturbations are shown in figure 5. These modes possess poloidal wave-numbers primarily within $k_\theta \sim \{0.1 \ldots 0.5\}\,\mathrm{cm}^{-1}$ ($k_\theta \rho_s \{0.01 \ldots 0.05\}$) and are linked to resistive PB modes, with filaments observed at $f \sim 2.3$ kHz and heat-load peaks on the outer divertor target ranging from $3.2 - 12\,\mathrm{MW\,m}^{-2}$.

The linearly stable modes, $n < 4$ and $n > 11$ later become non-linearly excited before unstable modes influence the background plasma due to three-wave interaction such that the growth rate of the driven mode is the sum of the driving modes ($\gamma_{k\pm m} = \gamma_k + \gamma_m$) [49]. The $v_{pol,mode}$ corresponds to the velocity for resistive PB modes. At the maximum amplitude location, the mode velocity is roughly $1\,\mathrm{km\,s}^{-1}$ in the ion diamagnetic direction. The perturbations are found to have smaller poloidal wave-number ($k_\theta \sim 0.1$ to $0.5\,\mathrm{cm}^{-1}$) than those in experimental discharges ($k_\theta \approx 0.6\,\mathrm{cm}^{-1}$). As the simulation transitions from linear to non-linear, the pedestal perturbations change in freq. from $\sim$40–13 kHz, where the latter approximately corresponds to the lower end of frequencies typically observed for the QCM in AUG [12].

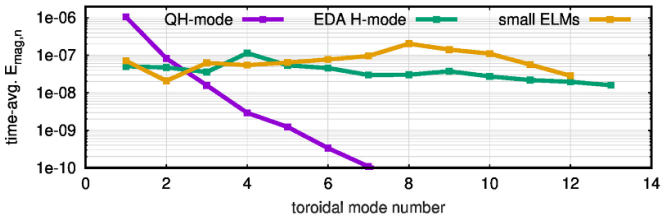

Figure 6. Comparison of the three small/no-ELM regimes at AUG in terms of the magnetic energy of each non-axisymmetric mode present. The simulation describing QH-mode was carried out with all toroidal mode numbers between $n = 0$ and 6, EDA H-mode between $n = 0$ and 13, and for this simulation of small ELMs between $n = 0$ and 12. The dominant mode in each simulation is different both in terms of the mode number as well as the mode structure.

3.5. Comparing simulations of small/no-ELMs in AUG

In the previous sections, the non-linear extended MHD simulations of three small/no-ELM regimes at AUG were presented. For both small ELMs at low triangularity and for the EDA H-mode, the underlying instabilities have strongest linear growth rates of medium-to-high toroidal mode numbers. These linearly dominant instabilities are dominantly ballooning in structure, i.e. strongly localised to the LFS, and display characteristics typical of resistive ballooning nature. Namely, the mode velocity and changes to the linear growth rates resulting from variations in local resistivity [37, 41]. In contrast, for the QH-mode linearly dominant is an $n = 2$ kink-peeling mode, which grows at a slower rate than the resistive PB modes that dominate the other two regimes. The $n = 2$ mode later on in the simulation becomes opaqued by the growth of an $n = 1$ kink-peeling mode that then saturates at a high amplitude and is the defining factor in the interaction between the axisymmetric background and the non-axisymmetric perturbations that form the EHO. Figure 6 shows the energy spectrum of each regime during the non-linear phase in logarithmic scale. For QH-mode, the energies of modes with higher toroidal harmonics in the non-linear phase decreases sharply with n.

During the non-linear phase of the QH-mode simulations, most energy is exchanged from the $n = 1$ towards modes with higher toroidal mode numbers. Conversely, for small ELMs at low triangularity and EDA H-mode, there is a much more active energy exchange between various different modes throughout the non-linear phase. For small ELMs, the dominant toroidal mode numbers during the linear phase and non-linear phase are medium-to-high n ($n = 7 \ldots 10$) with low-n modes becoming non-linearly destabilised. Similarly, for the EDA H-mode simulations, low-n ($n < 4$) become non-linearly excited once the linearly unstable modes grow to a sufficiently large amplitude. However, as the linearly most unstable modes begin to affect the axisymmetric background (they deplete the pedestal density), the non-linearly dominant modes begin to shift towards lower toroidal mode numbers.

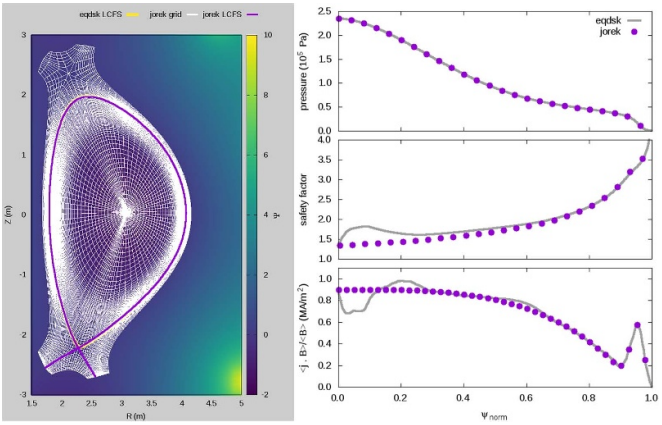

Figure 7. Set-up of JT-60SA scenario 4-1 with 4.6 MA and 2.26 T. (left) magnetic equilibrium and double x-point grid used in JOREK simulations. The separatrix from the imported equilibrium (yellow) is below that from the equilibrium solved with JOREK (purple). (right) pressure, safety factor, and current density profiles from the original equilibrium (gray lines) together with the profiles that go into JOREK.

4. Preliminary extended MHD simulations of JT-60SA

Using the capabilities of JOREK shown in AUG simulations of small/no-ELM scenarios towards future machines is important to probe for such regimes of operation before experimental discharges are possible. This undertaking carries several complications and uncertainties since it relies solely on integrated modelling results rather than input from experimental observations. The present section shows the most recent progress in this regard by presenting preliminary results for the pedestal dynamics in the JT-60SA tokamak, which is forming the basis for predictively studying the access and sustainment of different ELM and ELM-free scenarios in JT-60SA. The equilibrium and profiles are obtained from the JT-60SA scenario development team (scenario 4-1) with a plasma current of 4.6 MA, magnetic field on-axis 2.26 T, which is done with the GOTRESS+ code [50]. The pedestal analysis uses the EPED1 model with the coefficient related to the pedestal width of 0.076 [51]. Upon importing the equilibrium from the scenario development, JOREK internally solves the Grad-Shafranov equation which is then used to construct the flux-aligned grid. The resulting magnetic geometry is shown in figure 7(left), which includes a colour map of the imported equilibrium ψ, the double x-point grid used in JOREK, and the separatrix in purple (which overlaps with the separatrix from the imported equilibrium in yellow). Figure 7(right) shows the profiles of pressure, safety factor, and current density in grey for the equilibrium of the scenario development and in purple of the JOREK simulations.

The current density profile that is used for the JOREK simulations is slightly modified to describe a continuous curve in the core. This is done in order to avoid the appearance of numerical instabilities while the total integrated current is

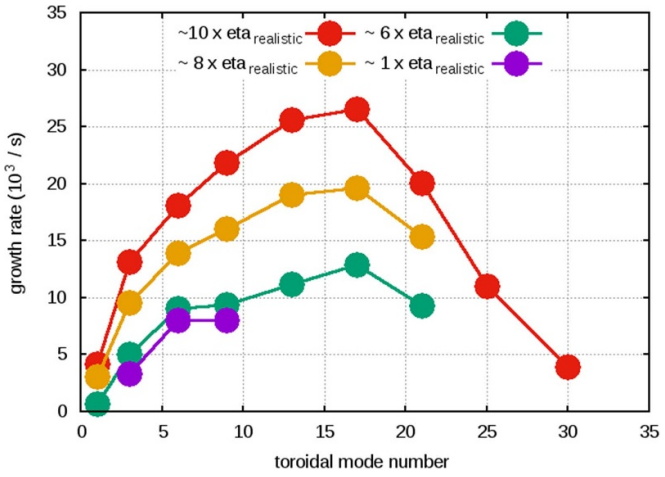

Figure 8. Linear growth rates for JT-60SA scenario 4-1 for a resistivity scan between nominal and high resistivity (≈10x realistic) using fully established diamagnetic and ExB flows.

kept at 4.6 MA. After the initialisation, equilibrium solve, and grid construction, the time-stepping begins and convection, sources, and diffusion start to set in. Upon an adequate choice of diffusion coefficients and sources, the density and temperature profiles describe a minor steepening of the pedestal and any changes in pedestal steepness has an effect on the current density through a bootstrap current source term. This approach at studying the destabilisation of pedestal instabilities through a build-up of the pedestal as was done in [22]. This approach at finding the onset of type-I ELMs allowed for the simulation of ELM cycles for the first time, and it self-consistently includes the influence of diamagnetic and ExB flows.

In the first stage of the simulation, only the axisymmetric $n = 0$ mode is considered until the full establishment of parallel and poloidal flows resulting from the boundary conditions at the divertor targets (Mach-1 conditions are chosen for the parallel velocity) and from the diamagnetic extension. Thereafter, non-axisymmetric perturbations with different toroidal mode numbers are initialised in order to probe for their linear stability (several simulations with a single toroidal mode number are carried out in order to do this). In the following, JOREK simulation results at different resistivities are shown and, thereafter, different diamagnetic drift values are investigated at nominal resistivity and high resistivity (≈10 times larger than nominal).

4.1. Probing linear stability of the pedestal

Simulations of JT-60SA are more challenging than AUG because of the larger device size and higher Lundquist number. At high resistivity (≈10 times the anticipated value given by Spitzer resistivity with neoclassical corrections and considering a Z_{eff} of 2.5 in the pedestal) and with fully established diamagnetic and ExB flows there are several linearly unstable modes, as shown in figure 8(red) with the most unstable mode corresponding to $n = 17$ in a scan of $n = 1$, 3, 6, 9, 13, 17, 21, 25, and 30. The perturbations of different toroidal mode numbers are initialised at noise level in simulations that consider

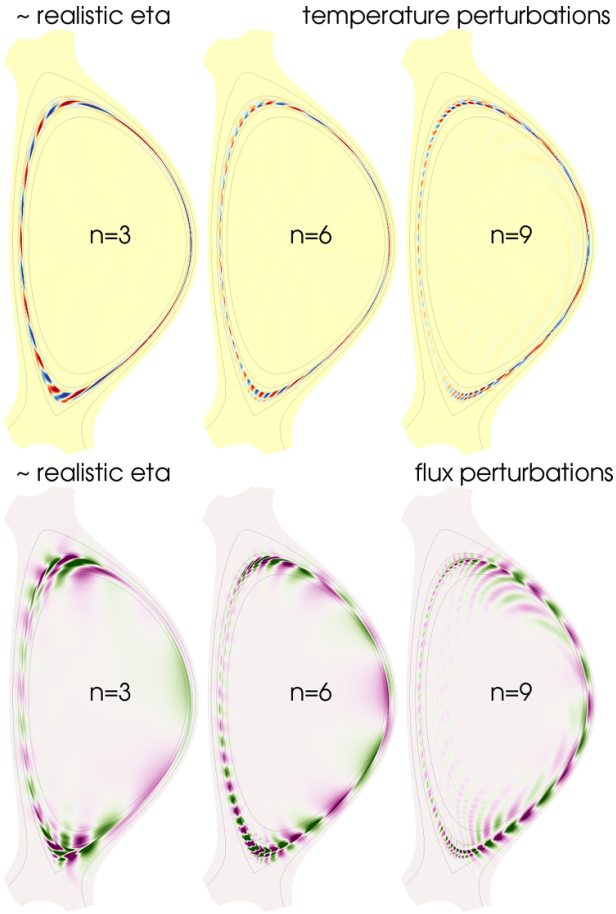

Figure 9. Mode structures shown for the perturbations in temperature (top) and poloidal magnetic flux (bottom) for the unstable modes ($n = 3$, 6 and 9) at nominal resistivity. Flux surfaces at $\psi_{\text{norm}} = 0.925$, 1.000, and 1.075 are included with thin gray lines.

the axisymmetric background and a single-n because the main interest at this stage is only the linear growth rates of different toroidal modes. Modelling the axisymmetric plasma background together with several harmonics goes beyond the scope for this paper, but will need to be accounted for in order to understand the non-linear interaction between the $n = 0$ background and the non-axisymmetric instabilities in the pedestal. Considering progressively smaller resistivity (i.e. moving towards more realistic values) results in a narrower mode spectrum. At realistic resistivity (purple in figure 8), the unstable modes are only $n = 3$, 6, and 9 (within the probed toroidal mode numbers). The perturbations caused by these modes in the temperature and the poloidal magnetic flux are shown in figure 9 top and bottom, respectively. From the figure it is possible to distinguish that $n = 3$ features a mostly peeling mode structure while the other two modes are distinguished by a mode structure of coupled PB modes.

4.2. Influence of flows on pedestal stability

Without diamagnetic and ExB flows, their stabilising effect on ballooning modes (which is strongest for modes with higher toroidal harmonics) is not accounted for, as shown in figure 10

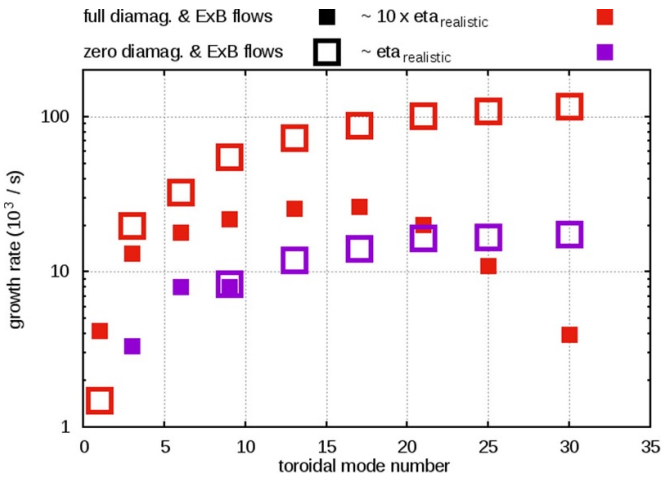

Figure 10. Linear growth rates for JT-60SA scenario 4-1 for simulations with high ($\approx 10x$ realistic, in red) and nominal resistivity (in purple) using fully established diamagnetic and ExB flows (full squares) and zero diamagnetic and ExB flows (open squares).

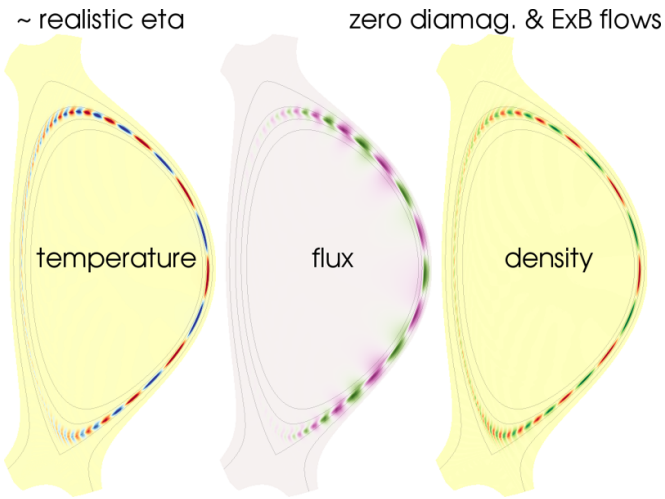

Figure 11. Mode structures shown for the perturbations in temperature (left), poloidal magnetic flux (centre), and density (right) for the $n = 9$ at nominal resistivity, but without the diamagnetic effects included. Flux surfaces at $\psi_{\mathrm{norm}} = 0.925$, 1.000, and 1.075 are included with thin gray lines. These perturbations have a dominant ballooning structure such that the HFS is mostly unperturbed.

for nominal resistivity (purple) and ≈ 10 times larger resistivity (red). It is found that at nominal resistivity, PB modes are unstable with full diamagnetic and ExB flows for $n = 3$, 6, and 9 (and their mode structure was shown in figure 9). When diamagnetic effects are neglected, modes with $n \geqslant 9$ are found to be unstable at nominal resistivity. The mode structure for $n = 9$ at nominal resistivity and without diamagnetic effects is shown in perturbations of the temperature, poloidal magnetic flux, and density in figure 11. The mode structure of the $n = 9$ mode shown in figure 9(right) can be compared its counterpart without the diamagnetic and ExB flows, which clearly shows that in the absence of flows, the poloidal mode structure is much more ballooning in nature and, therefore, has lost most of the peeling characteristics. This is because most of the stabilisation caused by flows is on high-m perturbations which are more predominantly ballooning in their structure. The fact that $n = 3$ and 6 are only unstable at nominal resistivity when the diamagnetic effects are taken into consideration is because of the destabilising effect that ExB and its shear have on low-n modes. The same happens for the $n = 1$ mode at high resistivity. This destabilisation of low-n modes with the inclusion of ExB flows and shear has been previously reported in [52, 53].

5. Conclusions

Bringing modelling activities of small/no-ELM regimes to a predictive status can be instrumental in determining operational windows of naturally ELM-free regimes in future devices. Such predictive results are very important for the progress of tokamak fusion in order to safely evaluate and design new devices at reactor-relevant scales because experimental scalings alone cannot determine safe operation windows for small/no-ELM regimes. In order to advance modelling capabilities towards such predictive realms it is necessary to first achieve robust validation studies that reproduce experimental results both qualitatively as well as, and most importantly, quantitatively. In this contribution, recent developments from the JOREK code that validate simulations with experimental results from ASDEX Upgrade were presented and contrasted, and predictive simulations for JT-60SA were described.

Simulations for three different small/no-ELM regimes in AUG (QH-mode, QCE regime, and EDA H-mode) were included and compared to experiments both qualitatively and quantitatively with an overall good agreement. An $n = 1$-dominated kink-peeling mode with higher harmonics saturates (the amplitude of the higher harmonics decays exponentially with toroidal mode number) and dominates the dynamics for QH-mode and is found to closely relate to the EHO in experiments. For the QCE regime and EDA H-mode, resistive PB modes are found to dominate the non-linear dynamics and reflect fluctuation frequencies within the expected ranges from experiments. The close connections found between simulations and experiment are encouraging observations that will help pave the way for more complete validations and ultimately predictive simulations, which have begun already for JT-60SA as detailed in this paper.

Predictive simulations of JT-60SA start from a magnetic equilibrium calculated by the scenario development team of JT-60SA. The equilibrium that is used has high shaping and low $n_{\mathrm{e,sep}}$. This equilibrium is fed to JOREK in order to probe the pedestal stability including the effect of non-zero resistivity, viscosity, and diamagnetic drift which are very important for the linear growth rates of different instabilities as well as the non-linear dynamics of pedestal instabilities and their interaction with the axisymmetric plasma background. A scan in the pedestal resistivity, which covered a range between the expected value all the way up to ten times that value. At high resistivity, a broad spectrum of modes between $n = 1$ and 30 was found to be unstable with the most unstable mode corresponding to $n = 17$. At realistic resistivity, however, the mode

spectrum turned much more narrow and included toroidal harmonics only between (and including) $n = 3$ and 9. The role of diamagnetic drifts was studied for JT-60SA both at high resistivity and at realistic resistivity, showing its important influence onto the stability of PB modes. In the simulations without diamagnetic drifts (which also means simulations with a very small ExB flow), low-n modes were found to be less unstable (or completely stable) than with the realistic diamagnetic and ExB flows. Non-linear investigations of the mode activity and interaction with the axisymmetric plasma background, as well as small/no-ELM regime access by probing different values of $n_{e,sep}$ and at lower plasma current is foreseen for future work.

Acknowledgments

This work has been carried out within the framework of the EUROfusion Consortium, funded by the European Union via the Euratom Research and Training Programme (Grant Agreement No. 101052200—EUROfusion). Views and opinions expressed are however those of the author(s) only and do not necessarily reflect those of the European Union or the European Commission. Neither the European Union nor the European Commission can be held responsible for them. In particular, A. Cathey received funding from a EUROfusion Researcher Grant and work package Tokamak Exploitation, and are acknowledged. The non-linear JOREK simulations were performed using the Marconi-Fusion supercomputer within the FUA37_MHD project.

ORCID iDs

A. Cathey https://orcid.org/0000-0001-7693-5556
M. Hoelzl https://orcid.org/0000-0001-7921-9176
L. Meier https://orcid.org/0009-0004-2705-1411
M.G. Dunne https://orcid.org/0000-0002-5259-9970
G.T.A. Huijsmans https://orcid.org/0000-0002-1435-4892
L. Gil https://orcid.org/0000-0002-9970-2154
G.F. Harrer https://orcid.org/0000-0002-1150-3987
N. Aiba https://orcid.org/0000-0002-0652-2892
D.J. Cruz-Zabala https://orcid.org/0000-0001-5925-5153
S.J.P. Pamela https://orcid.org/0000-0001-8854-1749
E. Viezzer https://orcid.org/0000-0001-6419-6848
E. Wolfrum https://orcid.org/0000-0002-6645-6882
S. Günter https://orcid.org/0000-0001-6924-209X

References

[1] Viezzer E. 2018 Access and sustainment of naturally ELM-free and small-ELM regimes *Nucl. Fusion* **58** 115002
[2] Zohm H. 1996 Edge localized modes (ELMs) *Plasma Phys. Control. Fusion* **38** 105
[3] Kirk A. *et al* 2006 Evolution of filament structures during edge-localized modes in the mast tokamak *Phys. Rev. Lett.* **96** 185001
[4] Eich T., Sieglin B., Thornton A.J., Faitsch M., Kirk A., Herrmann A. and Suttrop W. (JET contributors, MST contributors, ASDEX Upgrade and MAST teams) 2017 ELM divertor peak energy fluence scaling to ITER with data from JET, MAST and the ASDEX upgrade *Nucl. Mater. Energy* **12** 84–90
[5] Loarte A. *et al* 2014 Progress on the application of ELM control schemes to ITER scenarios from the non-active phase to DT operation *Nucl. Fusion* **54** 033007
[6] Viezzer E. *et al* (the EUROfusion MST1 Team and the ASDEX Upgrade team) 2021 Progress towards a quiescent, high confinement regime for the all-metal ASDEX upgrade tokamak *47th EPS Conf. on Plasma Physics*
[7] Burrell K.H. *et al* 2001 Quiescent double barrier high-confinement mode plasmas in the DIII-D tokamak *Phys. Plasmas* **8** 2153–62
[8] Labit B. *et al* 2019 Dependence on plasma shape and plasma fueling for small ELM regimes in TCV and ASDEX upgrade *Nucl. Fusion* **59** 086020
[9] Dunne M.G. 2023 private communication
[10] Greenwald M. *et al* 1999 Characterization of enhanced D_{alpha} high-confinement modes in alcator *C*-mod *Phys. Plasmas* **6** 1943–9
[11] Sun P.J. *et al* 2019 Experimental study of quasi-coherent mode using EAST tangential CO_2 laser collective scattering diagnostic in far-forward mode *Phys. Plasmas* **26** 012304
[12] Gil L. *et al* (Stationary ELM-free h-mode in ASDEX upgrade) 2020 *Nucl. Fusion* **60** 054003
[13] Futatani S., Cathey A., Hoelzl M., Lang P.T., Huijsmans G.T.A. and Dunne M. (the JOREK Team, the ASDEX Upgrade Team and the EUROfusion MST1 Team) 2021 Transition from no-ELM response to pellet ELM triggering during pedestal build-up—insights from extended MHD simulations *Nucl. Fusion* **61** 046043
[14] Cathey A., Hoelzl M., Futatani S., Lang P.T., Lackner K., Huijsmans G.T.A., Pamela S.J.P. and Günter S. (the JOREK Team, the ASDEX Upgrade Team and the EUROfusion MST1 Team) 2021 Comparing spontaneous and pellet-triggered ELMs via non-linear extended MHD simulations *Plasma Phys. Control. Fusion* **63** 075016
[15] Mitterauer V., Hoelzl M., Willensdorfer M., Dunne M., Schwarz N. and Artola J. (JOREK Team, ASDEX Upgrade Team and EUROfusion MST1 Team) 2022 Non-linear free boundary simulations of the plasma response to resonant magnetic perturbations in Asdex Upgrade plasmas *J. Phys.: Conf. Ser.* **2397** 012008
[16] Kim S.K. *et al* 2023 Transition in particle transport under resonant magnetic perturbations in a tokamak *Nucl. Fusion* **63** 106013
[17] Artola F.J., Huijsmans G.T.A., Hoelzl M., Beyer P., Loarte A. and Gribov Y. 2018 Non-linear magnetohydrodynamic simulations of edge localised mode triggering via vertical position oscillations in ITER *Nucl. Fusion* **58** 096018
[18] Hoelzl M. *et al* 2021 The JOREK non-linear extended MHD code and applications to large-scale instabilities and their control in magnetically confined fusion plasmas *Nucl. Fusion* **61** 065001
[19] Huysmans G.T.A. and Czarny O. 2007 MHD stability in x-point geometry: simulation of ELMs *Nucl. Fusion* **47** 659
[20] Pamela S.J.P. *et al* (JET Contributors) 2017 Recent progress in the quantitative validation of JOREK simulations of ELMs in JET *Nucl. Fusion* **57** 076006
[21] Orain F. *et al* 2015 Resistive reduced MHD modeling of multi-edge-localized-mode cycles in tokamak x-point plasmas *Phys. Rev. Lett.* **114** 035001
[22] Cathey A., Hoelzl M., Lackner K., Huijsmans G.T.A., Dunne M.G., Wolfrum E., Pamela S.J.P., Orain F. and Günter S. (the JOREK Team, the ASDEX Upgrade Team and the EUROfusion MST1 Team) 2020 *Nucl. Fusion* **60** 124007
[23] Burrell K.H., Osborne T.H., Snyder P.B., West W.P., Fenstermacher M.E., Groebner R.J., Gohil P., Leonard A.W. and Solomon W.M. 2009 Edge pedestal control in quiescent

H-mode discharges in DIII-D using co-plus counter-neutral beam injection *Nucl. Fusion* **49** 085024
[24] Snyder P.B. *et al* 2007 Stability and dynamics of the edge pedestal in the low collisionality regime: physics mechanisms for steady-state ELM-free operation *Nucl. Fusion* **47** 961–8
[25] Solomon W.M., Snyder P.B., Burrell K.H., Fenstermacher M.E., Garofalo A.M., Grierson B.A., Loarte A., McKee G.R., Nazikian R. and Osborne T.H. 2014 Access to a new plasma edge state with high density and pressures using the quiescent *h* mode *Phys. Rev. Lett.* **113** 135001
[26] Liu F., Huijsmans G.T.A., Loarte A., Garofalo A.M., Solomon W.M., Snyder P.B., Hoelzl M. and Zeng L. 2015 Nonlinear MHD simulations of quiescent H-mode plasmas in DIII-D *Nucl. Fusion* **55** 113002
[27] Liu F. *et al* 2017 Nonlinear MHD simulations of QH-mode DIII-D plasmas and implications for ITER high Q scenarios *Plasma Phys. Control. Fusion* **60** 014039
[28] King J.R., Kruger S.E., Burrell K.H., Chen X., Garofalo A.M., Groebner R.J., Olofsson K.E.J., Pankin A.Y. and Snyder P.B. 2017 MHD modeling of a DIII-D low-torque QH-mode discharge and comparison to observations *Phys. Plasmas* **24** 055902
[29] Pankin A.Y., King J.R., Kruger S.E., Chen X., Burrell K.H., Garofalo A.M., Groebner R.J., McKee G.R. and Yan Z. 2020 Towards validated MHD modeling of edge harmonic oscillation in DIII-D QH-mode discharges *Nucl. Fusion* **60** 092004
[30] Li Z. *et al* (DIII-D Team) 2022 Numerical modeling of pedestal stability and broadband turbulence of wide-pedestal QH-mode plasmas on DIII-D *Nucl. Fusion* **62** 076033
[31] Meier L. *et al* 2023 *Nucl. Fusion* **63** 086026
[32] Oyama N. *et al* (the ITPA Pedestal Topical Group) 2006 Pedestal conditions for small ELM regimes in tokamaks *Plasma Phys. Control. Fusion* **48** A171–81
[33] Sartori R. *et al* 2004 Study of type III ELMs in JET *Plasma Phys. Control. Fusion* **46** 723
[34] Garcia J. *et al* 2022 New H-mode regimes with small ELMs and high thermal confinement in the Joint European Torus *Phys. Plasmas* **29** 032505
[35] Harrer G.F. *et al* 2018 Parameter dependences of small edge localized modes (ELMs) *Nucl. Fusion* **58** 112001
[36] Faitsch M., Eich T., Harrer G.F., Wolfrum E., Brida D., David P., Griener M. and Stroth U. 2021 Broadening of the power fall-off length in a high density, high confinement H-mode regime in ASDEX upgrade *Nucl. Mater. Energy* **26** 100890
[37] Cathey A., Hoelzl M., Harrer G., Dunne M.G., Huijsmans G.T.A., Lackner K., Pamela S.J.P., Wolfrum E. and Günter S. (the JOREK Team, the ASDEX Upgrade Team and the EUROfusion MST1 Team) 2022 MHD simulations of small ELMs at low triangularity in ASDEX upgrade *Plasma Phys. Control. Fusion* **64** 054011
[38] Grenfell G. *et al* 2024 The multi-faced nature of the quasicoherent mode in EDA H-mode *Nucl. Fusion* submitted
[39] Kalis J. *et al* (the ASDEX Upgrade Team and the EUROfusion MST1 Team) 2023 Experimental characterization of the quasi-coherent mode in EDA H-mode and QCE scenarios at ASDEX upgrade *Nucl. Fusion* **64** 016038
[40] Kallenbach A. *et al* (EUROfusion MST1 team) 2020 Developments towards an ELM-free pedestal radiative cooling scenario using noble gas seeding in ASDEX upgrade *Nucl. Fusion* **61** 016002
[41] Cathey A. *et al* (the JOREK Team, the ASDEX Upgrade Team and the EUROfusion MST1 Team) 2023 Probing non-linear MHD stability of the EDA H-mode in ASDEX upgrade *Nucl. Fusion* **63** 062001
[42] Groebner R.J., Burrell K.H. and Seraydarian R.P. 1990 Role of edge electric field and poloidal rotation in the L-H transition *Phys. Rev. Lett.* **64** 3015–8
[43] Cavedon M. *et al* (the ASDEX Upgrade Team) 2017 Pedestal and E_r profile evolution during an edge localized mode cycle at ASDEX upgrade *Plasma Phys. Control. Fusion* **59** 105007
[44] Rogers B.N. and Drake J.F. 1999 Diamagnetic stabilization of ideal ballooning modes in the edge pedestal *Phys. Plasmas* **6** 2797–801
[45] Sauter O., Angioni C. and Lin-Liu Y.R. 1999 Neoclassical conductivity and bootstrap current formulas for general axisymmetric equilibria and arbitrary collisionality regime *Phys. Plasmas* **6** 2834–9
[46] Sauter O., Angioni C. and Lin-Liu Y.R. 2002 Erratum: 'Neoclassical conductivity and bootstrap current formulas for general axisymmetric equilibria and arbitrary collisionality regime' [Phys. Plasmas 6, 2834 (1999)] *Phys. Plasmas* **9** 5140–2839
[47] Suttrop W. *et al* (the ASDEX Upgrade Team and contributors to the JET-EFDA workprogramme) 2005 Studies of the 'Quiescent H-mode' regime in ASDEX Upgrade and JET *Nucl. Fusion* **45** 721–30
[48] Wolfrum E. *et al* 2011 Characterization of edge profiles and fluctuations in discharges with type-II and nitrogen-mitigated edge localized modes in ASDEX upgrade *Plasma Phys. Control. Fusion* **53** 085026
[49] Krebs I., Hoelzl M., Lackner K. and Günter S. 2013 Nonlinear excitation of low-n harmonics in reduced magnetohydrodynamic simulations of edge-localized modes *Phys. Plasmas* **20** 082506
[50] Honda M., Aiba N., Seto H., Narita E. and Hayashi N. 2021 Development of a novel integrated model GOTRESS+ for predictions and assessment of JT-60SA operation scenarios including the pedestal *Nucl. Fusion* **61** 116029
[51] Snyder P.B., Osborne T.H., Burrell K.H., Groebner R.J., Leonard A.W., Nazikian R., Orlov D.M., Schmitz O., Wade M.R. and Wilson H.R. 2012 The EPED pedestal model and edge localized mode-suppressed regimes: studies of quiescent H-mode and development of a model for edge localized mode suppression via resonant magnetic perturbationsa) *Phys. Plasmas* **19** 056115
[52] Xu G.S. *et al* 2017 E × B flow shear drive of the linear low-*n* modes of EHO in the QH-mode regime *Nucl. Fusion* **57** 086047
[53] Chen J.G., Xu X.Q., Ma C.H., Xi P.W., Kong D.F. and Lei Y.A. 2017 Impact of E × B shear flow on low-n MHD instabilities *Phys. Plasmas* **24** 050704